Formation of extended topological defects during symmetry breaking phase transitions in O(2) and O(3) models

G. Holzwarth*
Fachbereich Physik, Universität Siegen, D-57068 Siegen, Germany
(Received 14 January 1999; published 26 April 1999)

The density of extended topological defects created during symmetry breaking phase transitions depends on the ratio between the correlation length in the symmetric phase near T_c and the winding length of the defects as determined by the momentaneous effective action after a typical relaxation time. Conservation of winding number in numerical simulations requires a suitable embedding of the field variables and the appropriate geometrical implementation of the winding density on the discrete lattice. We define a modified Kibble limit for the square lattice and obtain defect densities as functions of winding lengths in O(2) and O(3) models. The latter allows one to observe the formation of disoriented aligned domains within the easy plane. Their extent is severely limited by the momentaneous defect density during the course of the quench.
[S0556-2821(99)06110-X]

PACS number(s): 11.27.+d, 05.45.Yv, 12.39.Dc, 64.60.Cn

I. INTRODUCTION

The formation of defects during symmetry breaking phase transitions has found increasing attention in a variety of applications ranging from condensed matter systems to cosmological scenarios [1]. The idea to consider baryons as topological defects in an N-component chiral meson field Φ_i constrained by $\Phi^2=\text{const}$ [2] similarly has initiated attempts to estimate multiplicities of baryon and antibaryon production in high energy events or heavy ion collisions from the dynamics of defect formation during the cooling phase of an expanding hot hadronic gas [3,4]. There are strong theoretical indications that during this cooling process the chiral O(N) symmetry is spontaneously broken near a critical temperature T_c, and since the critical temperature is estimated to be of the order of the pion mass m_π ([5] and references therein), it may appear sufficient to describe this chiral transition in the framework of low-energy effective theory for the mesonic fields Φ_i [6]. However, perturbative methods for the evaluation of the relevant effective potential near the critical temperature are probably not very reliable; the role eventually played by other degrees of freedom is not really understood, so at present it is not even clear whether this chiral transition would be first or second order (see, e.g., the discussion in [7,8]).

In analogy with phenomena observed in condensed matter systems there also have been speculations about the simultaneous ocurrence of extended domains with different average orientation of the aligned field [''disoriented chiral condensate'' (DCC)] which rearrange into a uniform vacuum on a much longer time scale and therefore could manifest themselves through anomalous branching ratios for the production of differently charged mesons [9]. Evidently, the existence of differently oriented domains and defect formation are intimately related, especially if the defects are of topological type which cannot simply disappear from a field configuration by local unwinding.

Depending on the physical system under consideration the nature of the defects is determined by the choice of the manifold on which the fields live [10]: If the constraint $\Phi^2=\text{const}$ is enforced, the fields live on the $(N-1)$-dimensional sphere S^{N-1}, conveniently parametrized by angular variables. This embedding can provide defects with a topologically protected winding number and thus in case of the chiral field allows to identify them with baryons.

Near the phase transition, however, it may be appropriate to relax the constraint and allow all N components of Φ to move independently. Then a Euclidean R^N embedding appears most convenient and in fact, the possible formation of DCC's in the chiral phase transition has been investigated in this framework [11]. The winding number of a field configuration embedded in R^N is, however, not topologically conserved: it will undergo discrete changes, if at some spacetime point all field components vanish, i.e., if the field configuration moves across the origin $\Phi^2(x)=0$.

In order to preserve the identification of winding number with baryon number it is necessary to insist on the angular nature of the chiral field, while the additional degree of freedom is picked up by the modulus $|\Phi|$, the scalar σ field. In other words, the topologically trivial R^N embedding is replaced by the $R^1\times S^{N-1}$ manifold with nontrivial homotopy group Z. Here the origin $\Phi=0$ is excluded as a highly singular branch point where different angular sheets are tied together. Any field configuration which moves across this point, leaves a defect or antidefect of winding number ± 1 at the spatial position where this happens, which remains connected to the rest of the moving field by a string. The spatial structure of string and defect are determined by the dynamics of the classical field. The nontrivial structure of the modulus of Φ along the string constitutes the ''bag,'' which interpolates from the vacuum value of the σ field surrounding the defect to a (small) value in its center where the angular fields change rapidly from one sheet to the next. For a simple $(1+1)$-dimensional O(2) model this has been discussed in detail in [12].

*Email address: holzwarth@physik.uni-siegen.de

These considerations naturally pose two questions: How do different embeddings affect the average multiplicities of defects and antidefects and the possible existence of disoriented domains during the chiral transition? What is the influence of the spatial structure of the topological defects (as determined by the temperature-dependent effective action) on their production multiplicities and on the possible formation of large extended disoriented domains?

One may hope that for the essential features of defect formation the order of the transition is not very important. If the transition is first order then it would proceed through nucleation of bubbles [13], which in their interior are characterized by an aligned chiral field with nonvanishing average value $\langle|\Phi|\rangle = f_0(T_c)$ of the chiral field as determined through the nontrivial minimum of the effective potential near T_c. The orientation of the aligned field in different bubbles could be considered as random, so the average distance of their centers can be taken as an initial correlation length $\xi(T_c)$ at T_c. This length provides the relevant scale for defect formation, irrespective of its physical size. On this scale the total volume V considered can be identified with the total number of bubble seeds near T_c. Growth and coalescence of bubbles then leads to the formation of topological defects within a typical formation time τ characteristic for the damping of local fluctuations.

Decisive for the multiplicity of the created defects is the ratio between their spatial extent, i.e., the ''radius'' or ''winding length'' l_W of the defects at the time of their formation and the correlation length $\xi(T_c)$. The winding length is determined by the stabilization mechanism supplied through the effective action for the average field.

If the winding length l_W is much smaller than the correlation length the defects can be considered as pointlike on the scale $\xi(T_c)$. Then the purely combinatorial rules [14] of random lattices apply for their formation, i.e., their average density n is given by the Kibble limit

$$n = (N_+ + N_-)/V = \frac{1}{2}\ (2)^{-D}\ \lambda_D, \tag{1}$$

where $(N_+ + N_-)$ is the number of defects plus antidefects, D is the space dimension, and the factor λ_D is the average ratio of the numbers of D simplices and vertices in a large random lattice, i.e., $\lambda_1 = 1, \lambda_2 = 2, \lambda_3 = \frac{24}{35}\pi^2$, etc. [15]. In this case the random field fluctuations during the typical time τ get transformed into a rather dense ensemble of defects and antidefects. These may become diluted in the following due to annihilation processes on a much larger time scale.

If, however, the value of the winding length l_W is larger than the average distance of the bubble seeds, then stabilization dynamics will prevent the formation of pointlike defects and antidefects inside the volume occupied by large extended stable defects or antidefects and Eq. (1) has to be replaced by

$$n = (N_+ + N_-)/V = \frac{1}{2}\ \left(2\frac{l_W}{\xi}\right)^{-D}\ \lambda_D, \tag{2}$$

i.e., before they have a chance to form, point defects and antidefects get instantly (i.e., within time τ) eaten by big stable solitons which carry the net winding number of the chiral field within the volume occupied by them. The formation of these large extended solitons is a direct process which does not proceed through multiple annihilations of smaller defects.

If for a sudden quench ($t_Q \ll \tau$) the effective potential at $T=0$ is established before any dynamical or dissipative mechanism can affect the initial random field configuration then the winding length $l_W(T)$ near $T=0$ will be relevant for the size of the ''cold'' defects formed. With the relevant scale still given by the initial correlation length or average bubble distance $\xi(T_c)$ near T_c, the ratio $l_W(T=0)/\xi(T_c)$ will enter into Eq. (2).

If typical quench times are much larger than the formation time ($t_Q \gg \tau$) then the number of initially created defects and antidefects will be given by Eq. (2) with winding length l_W characteristic for $T \approx T_c$. Subsequent changes in the defect multiplicities during the continuation of the quench depend on the scaling behavior of their winding length: if $l_W(T)$ decreases with the decreasing temperature [as in three spatial dimensions where l_W scales like $f_0(T)^{-1}$] then the (initially small) number of (initially large) defects stays small, so the multiplicity remains near the ratio $l_W(T_c)/\xi(T_c)$ in (2). On the other hand, if $l_W(T)$ increases during the quench [as in one spatial dimension where l_W scales like $f_0(T)^{1/2}$], the growing defects swallow many of the defect-antidefect pairs, so at the end of the slow quench the resulting multiplicities are the same as for a sudden quench, i.e., determined by the ratio $l_W(T=0)/\xi(T_c)$.

If the transition is second order no bubbles appear and the average distance between bubbles should be replaced by an instantaneous correlation length $\xi(T)$. For finite rate of cooling $\xi(T)$ remains finite near T_c because critical slowing down prevents response over large distances [16]. On the other hand $f_0(T)$ stays close to zero which (in 3 dimensions) implies large l_W. So also in this case the relevant winding lengths may exceed the pertinent correlation length of the plasma, so defect multiplicities can be much smaller than the limiting value given by Eq. (1).

Defect formation is intimately related with the size of DCC domains. If the transition proceeds in a way as to form a dense gas of pointlike defects and antidefects according to the Kibble limit (1), then domains of topologically trivial mesonic field which fill the remaining space between the different defects consequently have to be small (in units of ξ). With increasing ratio l_W/ξ the number of defects created decreases rapidly according to Eq. (2), but the chiral field in the spatial domains separating the defects is correlated due to the large winding length of the defects which ''organize'' the field surrounding them. In both limiting cases there seems to be little room for large (in units of ξ) domains of aligned but randomly oriented locally trivial field configurations. The actual physical size of these domains, of course, still depends on the magnitude of the basic length scale ξ in physical units; this, naturally, depends on the physical system considered and on the order of the transition. For the hot chiral gas in the chirally symmetric phase above T_c numbers for ξ typi-

cally quoted range from 0.5 fm to 1 fm. On a lattice with a lattice constant of that size individual ''cold'' baryons will cover just one lattice unit or less, while on formation near T_c the ''melted'' baryons [17] may smoothly extend over a large number of cells. We therefore expect a situation where the above considerations about the relevance of the winding length typically apply.

For a discussion of the chiral phase transition in the framework of effective meson fields it is therefore necessary to embed the fields in a manifold which allows for the topological protection of winding number, i.e., to use a separation into angular field variables and one modulus σ field. Practically, in lattice simulations, where topological arguments no longer apply, conserving algorithms have to be used for the updating of configurations during their evolution. We will describe the results of such simulations for the $1D$-O(2) model in Sec. II, and for the $2D$-O(3) model in Sec. III. It is expected that the bias introduced into the initial configurations through explicit chiral symmetry breaking provides another efficient mechanism to suppress defect formation [18]. This effect should be discussed in connection with the evolution of the σ field. We shall concentrate here on the interplay between winding length and defect densities. Because the winding length is mainly determined by the dynamics of the angular field variables we postpone a detailed discussion of features related to the evolution of the modulus σ field and, correspondingly, use unbiased initial configurations only.

II. O(2) MODEL IN 1+1 DIMENSIONS

Some of these features can be nicely visualized in the simple O(2) model in $1+1$ dimensions. As discussed above we concentrate here on the relation between winding length and defect density. To define the notation and for completeness we repeat some facts discussed in [12] concerning the topologically trivial R^2 vs nontrivial $R^1\times S^1$ embedding. Defects arise as stable static solutions for the effective Lagrangian density taken in the standard Φ^4 form (summation over $a=1,2$ and $\mu=0,1$ understood)

$$\mathcal{L}_0(\Phi)=\frac{1}{2}\partial_\mu\Phi_a\partial^\mu\Phi_a+\frac{\lambda_c}{4}(\Phi^2-f^2)^2-H\Phi_1. \qquad (3)$$

The term $H\Phi_1$ in Eq. (3) breaks chiral O(2) symmetry explicitly. In order to keep the minimum of the potential for finite H at the H-independent value $\Phi^2=f_0^2$ we define

$$f^2=f_0^2-\frac{H}{\lambda_c f_0}. \qquad (4)$$

In accordance with conclusions from 1-loop renormalization group applied to Eq. (3) we will take λ_c and H as temperature independent, while $f_0(T)$ decreases as T rises from $T=0$ towards $T=T_c$.

The Cartesian components $\Phi_{1,2}$ $(-\infty<\Phi_{1,2}<\infty)$ define the Euclidean R^2 embedding of this model, while modulus field σ and the angular variable ϕ $(0<\sigma<\infty, -\infty<\phi<\infty)$ related to Φ_i through

$$\Phi_1(x,t)=\sigma(x,t)\cos\phi(x,t),\quad \Phi_2(x,t)=\sigma(x,t)\sin\phi(x,t) \qquad (5)$$

define the embedding into the $S^1\times R^1$ manifold. The σ and π masses corresponding to these fields are

$$m_\pi^2=\frac{H}{f_0},\quad m_\sigma^2=2\lambda_c f_0^2+m_\pi^2. \qquad (6)$$

A convenient unit for dimensionful quantities is the temperature-independent symmetry breaker H of mass dimension 2. So, in the following, if numbers are given for dimensionful quantities, they are to be multiplied by appropriate powers of H.

In the Euclidean R^2 embedding the static part of Eq. (3) leads to stable nontopological solitons as long as the inequality

$$f_0^3\frac{\lambda_c}{H}>21.28 \qquad (7)$$

is satisfied. Otherwise, the only stable solution is the trivial ground state $\Phi_1\equiv f_0$, $\Phi_2\equiv 0$. This corresponds to approximately $m_\sigma>6.6\ m_\pi$, as stability condition. For a typical coupling strength $\lambda_c/H=60$ (which we use in the following) this implies $m_\pi<1.2$. On the other hand, in $R^1\times S^1$, the winding number B of topologically nontrivial field configurations with fixed angular boundary conditions $\phi(\pm\infty,t)=2\pi n_\pm$, $(n_\pm:\text{integer})$

$$B=\frac{1}{2\pi}\int_{-\infty}^{\infty}\frac{\partial}{\partial x}\phi(x,t)dx=n_+-n_-, \qquad (8)$$

is topologically conserved. For values of $f_0(T)$ below the limiting value (7) the angular field ϕ of nontrivial static configurations collapses into pointlike defects at some position $x=x_0$, while the modulus field σ describes a spatially extended ''bag'' profile satisfying

$$\sigma''-\lambda_c\sigma(\sigma^2-f^2)+H=0 \qquad (9)$$

$$\text{with}\ \ \sigma(x\to x_0)\to+0,\ \text{and}\ \ \sigma(|x|\to\infty)\to f_0.$$

The radius of this bag scales approximately like π/m_σ. Therefore, with f_0 small near T_c, where the stability condition (7) is not satisfied and the angular field collapsed to a point defect, the bag radius still is comparable to the angular winding length $l_W\approx\pi/m_\pi$ of the soliton, which solves the static O(2) model (3), if the constraint $\Phi^2\equiv f_0^2$ is enforced, i.e., if we simply consider a U(1) model on a circle S^1.

On the other hand, if the stability condition (7) is satisfied, the static solutions of the O(2) model in R^2 and in $R^1\times S^1$ embedding coincide. Because the modulus field of these configurations stays close to f_0, the corresponding angular field essentially also coincides with the soliton of the model constrained to the circle S^1 with $\sigma\equiv f_0$.

Statistical ensembles of these stable solutions are expected at the end of a cooling process that evolves from an initial ensemble of random configurations with correlation length ξ. The quench is defined through the variation of

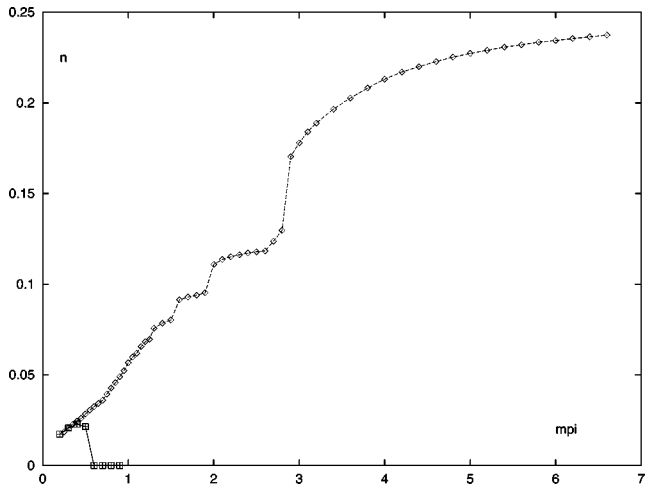

FIG. 1. Defect plus antidefect density $n=(N_+ + N_-)/N_L$ averaged over an ensemble of 100 random initial configurations on an $N_L=1000$ lattice after a sudden quench as function of inverse winding length m_π for the nonlinear O(2) model. The squares in the lower left corner show the same observable for the linear O(2) model in R^2 embedding.

$f_0(T)$ with time. For a numerical simulation the initial configurations before the onset of the quench we choose Gaussian deviates in the field components $\Phi_{1,2}(i)$, at the points $x_i = i\ \xi\ (i=0,\ldots,N_L)$ of a spatial grid of total length $L = N_L\xi$ with lattice constant ξ which defines the correlation length or distance of bubble seeds near T_c. Periodic boundary conditions are imposed by choosing $\Phi_{1,2}(0)=\Phi_{1,2}(N_L)$. From these random values of the Cartesian field components the initial configuration of the angular field $\phi(i)$ is obtained by taking the shortest path from the angle at point x_i to the angle at a neighboring point x_{i+1}. This guarantees that the absolute value of the increment in the angle from one point to the next is always less than π. Due to the periodic boundary conditions in the Cartesian field components the difference in the angular field $\phi(N_L)-\phi(0)$ then is an integer multiple of 2π, which defines the winding number B of that particular random initial configuration.

As we discussed above the winding length of nontrivial solutions in different embeddings is similar to the winding length of the model with the modulus of Φ constrained to $\Phi^2 \equiv f_0^2(T)$. The essentials of the relation between defect winding length and defect density therefore can also be observed within the simple U(1) [or nonlinear O(2)] model. As an example we consider the sudden quench where the initially prepared configurations are exposed at time $t=0$ to the effective action with constant $f_0(T=0)$. Then, within relaxation time τ, the configurations evolve into an ensemble of stable defects with winding length $l_W \approx \pi/m_\pi = \pi(f_0/H)^{1/2}$. In Fig. 1 the average final density n of defects plus antidefects averaged over an ensemble of 100 random initial configurations selected with total winding $B=0$ on an $N_L=1000$ lattice is plotted against the symmetry-breaking mass m_π.

The region where m_π is less than π is essentially characterized by a linear rise of the density n as expected from Eq. (2) for $D=1$. Beyond this value the winding length becomes comparable to the lattice constant ξ and we observe the onset of saturation with n slowly converging towards the Kibble limit (1) of $n=0.25$ (for $D=1$). A peculiar feature is that the increase in the number of finally surviving defects and antidefects with decreasing winding length proceeds in quite well-defined plateaus which are very robust against details of the evolution algorithm. Note that the absolute number of defects in the ensemble underlying Fig. 1 is rather large: e.g., in the sudden decrease of n just below $m_\pi=2.9$ a total average number of 0.05×10^5 defects are eaten by a tiny increase of the winding length, while in the region $(2.1\leqslant m_\pi \leqslant 2.8)$ mainly empty space in between defects is reduced. Evidently, this is an indication of a lattice effect: as we have noted, if m_π drops below π the defects start to grow beyond one lattice unit. As expected, for very small values of m_π the average density is again rather smooth. Altogether, we may conclude that the experiment confirms the expectation expressed in Eq. (2).

The squares connected by a full line in the left lower corner of Fig. 1 show average defect densities as calculated in the unconstrained O(2) model in Euclidean R^2 manifold. The theoretical limit of defect stability here (for $\lambda_c=60$) is close to $m_\pi \approx 1.2$. However, in the finite lattice calculation the defects disappear already near $m_\pi \approx 0.6$. Beyond that value the resulting defect densities are zero, while in the region of stability the average densities closely follow the linear rise as obtained in the U(1) model. Irrespective of the stability condition, for the unconstrained O(2) model embedded in $R^1\times S^1$, the defect densities are similar to those of the U(1) model for all values of m_π. However, in the region of instability where Eq. (7) is violated, average multiplicities in $R^1\times S^1$ embedding slightly exceed the U(1) results due to the smaller size of the radial bag (depending on the choice of λ_c) [cf. Eq. (6)].

Relations between winding length l_W of defects and formation of DCC domains cannot be addressed within the O(2) model, because the strength of the symmetry breaker necessary for finite l_W prevents local alignment in random directions. Outside the range of the defects the angle ϕ stabilizes always at multiples of 2π. We therefore turn to the O(3) model whose additional freedom allows to at least discuss partial aspects of DCC formation.

III. NONLINEAR O(3) MODEL IN 2+1 DIMENSIONS

Corresponding to our discussion of the constrained O(2) model we consider in this section only that version of the O(3) model where the modulus of Φ is constrained to a fixed value f_0. In two spatial dimensions f_0 is of mass dimension 1/2, so we use appropriate powers of f_0^2 as units for all dimensionful quantities. Then the fields Φ are unit vectors $\hat{\Phi}$ which live on the sphere S^2 and conveniently are parametrized by two angles θ and ϕ:

$$\Phi_1(\mathbf{x},t) = \cos\phi(\mathbf{x},t)\sin\theta(\mathbf{x},t),$$

$$\Phi_2(\mathbf{x},t) = \sin\phi(\mathbf{x},t)\sin\theta(\mathbf{x},t),$$

$$\Phi_3(\mathbf{x},t) = \cos\theta(\mathbf{x},t). \tag{10}$$

If $\hat{\Phi}$ converges towards a fixed unit vector, say $\hat{e_3}$, for spatial infinity on R^2 (sufficiently fast for the energy to converge) then the configuration space for smooth fields is disconnected due to the nontriviality of the second homotopy group $\pi_2(S^2)=Z$. Individual configurations then are characterized by the winding number B and local winding density ρ:

$$B=\int \rho \ d^2x, \tag{11}$$

$$\rho \equiv \frac{1}{8\pi}\epsilon_{ij}\hat{\Phi}\cdot(\partial_i\hat{\Phi}\times\partial_j\hat{\Phi}) \tag{12}$$

(summation over spatial indices i,j understood).

We consider the effective energy functional

$$\mathcal{E}[\hat{\Phi}]=\int \left(\frac{1}{2}\partial_i\hat{\Phi}\cdot\partial_i\hat{\Phi}+\lambda^2 \ \rho^2+\frac{1}{2\lambda^2}\ (\hat{\Phi}-\hat{e}_3)^2\right)d^2x. \tag{13}$$

Evidently, λ serves to scale the spatial extension of stable solutions, as it can be eliminated by $x\to\lambda x$. Both terms in $\mathcal{E}$, the ρ^2 (''Skyrme'') term and the explicitly symmetry-breaking last term, are necessary to stabilize solitons (the ''baby skyrmions'' [19]) with fixed winding length $l_W\propto\lambda$. For our present purpose to study the relation between l_W and average defect densities created in a symmetry breaking transition it is therefore sufficient to impose the quench through an appropriate time dependence of λ.

Discretizing the spatial coordinates to a two-dimensional lattice, the limit $\lambda\ll 1$ will produce defects which are point-like on the scale of the lattice constant, while $\lambda\gg 1$ will create smooth density distributions which extend over many lattice units. A characteristic problem arises in numerical simulations on a discrete lattice if the spatial extent of solitons is of the order of a few lattice constants or even less: this implies that differences in the angles θ and ϕ between neighboring lattice points may be of the order of π. In that case the definition (12) for the winding density ρ no longer applies. It is only for infinitesimally small differentials that the surface element $d\Omega$ on S^2 which is the image of the elementary lattice cell d^2x is given by $d\Omega=4\pi\rho \ d^2x$. But it is essential to maintain also for finite lattice constants the geometrical meaning of $d\Omega$ as the surface area which the image of the unit lattice cell cuts out from S^2. This can be readily implemented by defining $2\pi\rho$ as the (oriented) area of the spherical triangle which is cut out on S^2 by the three geodesics which connect the end points of three $\hat{\Phi}$ vectors attached to three corners of an elementary lattice cell. This works for arbitrary relative orientations of these $\hat{\Phi}$ vectors and allows even to detect one complete soliton inside one elementary lattice cell.[1] Clearly, this definition reduces to Eq. (12) in the continuum limit. Periodic boundary conditions (which compactify R^2 to a torus), or $\hat{\Phi}\to\hat{e}_3$ (which compactifies R^2 to S^2) then lead to integer values of the total winding number B obtained by summing up all oriented spherical triangles.

The topological considerations which guarantee conservation of B for continuous fields do not hold on the discrete lattice, because $\hat{\Phi}$ vectors attached to neighboring points on the lattice can differ arbitrarily. However, B conservation can easily be reimplemented into the evolution of the configurations by allowing in each updating step only configurations[2] which conserve B. In fact, this is a convenient way to compare evolutions which conserve B with others that allow for local unwinding of defects [20]. So it is also not necessary to introduce specific types of potentials (see, e.g., [21]) into Eq. (13) to avoid the ''exceptional'' configurations [22] as doorways for unwinding.

For the first term in Eq. (13) there is no similar compulsory extension to finite lattice constants because it is not of geometrical nature. So, as usual we just interpret it as nearest neighbor interaction.

Having thus defined the implementation of the model (13) on a discrete lattice which conserves those features essential for our present purpose, it remains to specify the initial configurations before the onset of the quench. Again we postpone here the question of any possible bias which may exist in these initial sets due to explicit symmetry breaking. Instead we choose a uniformly random set of $\hat{\Phi}$ vectors on all interior lattice points. Only on the boundaries we impose $\hat{\Phi}=\hat{e}_3$, i.e., $\theta=0$ with random ϕ.

In the following sense this initial random set realizes the maximal average number of defects which can be accommodated on this square lattice: First it should be noted that by definition of our map (which maps a triangle formed by two adjoining orthogonal lattice links and the diagonal connecting their end points onto the interior of the *smaller* of the two complementary spherical triangles formed by the corresponding geodesics on S^2) the image triangle covers always *less* than half of the sphere, and thus by definition does not contain a defect. So, this is different from the Kibble mechanism which allows for defects inside elementary triangles by considering an additional lattice point inside the triangle. However, if we add the (oriented) areas covered by the two adjoining images of both triangles which make up the elementary square lattice cell then it may happen that this sum

[1] In other words, we use a triangulation of the plane in terms of the triangles formed by two adjoining lattice links and one diagonal in each square lattice cell. Depending on the choice of the diagonal in the unit cell the area covered by the image of that cell on S^2 may differ by $\pm 4\pi$, i.e., the winding number may differ by ± 1. However, for the ensemble average, this is not relevant.

[2] Practically, in a local updating procedure this requires to control the sum of ρ only in the local vicinity of the points which are affected by the update.

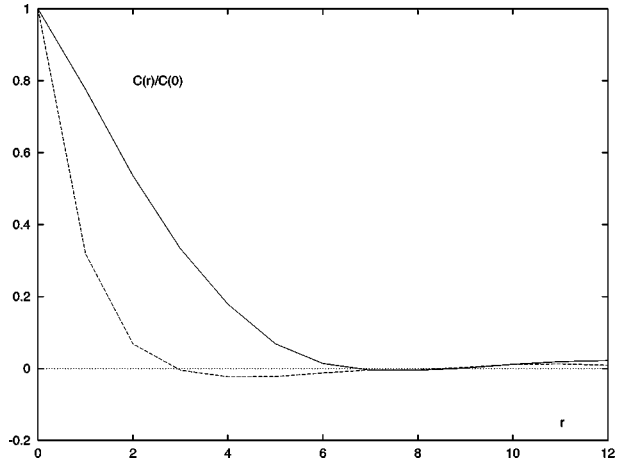

FIG. 2. Correlation function (15) $C(r)/C(0)$ for fast ($t_Q=10$) (dashed line) and slow ($t_Q=200$) (full line) quench near $\lambda\approx 3$.

covers more than half of the sphere, and by definition we then may count that as one defect inside this elementary lattice cell. In fact, if λ is very small, such a configuration will rapidly evolve into a configuration where the sum of these two spherical triangles (which represent the image of the lattice cell) is close to 4π. We may call this the Kibble limit for the square lattice. It differs from the triangular limit (1) by a factor 1/4 (in two dimensions), which we interpret as a difference in the definition of the correlation length ξ by a factor of two for uniformly random configurations on the vertices of a square lattice, as compared to the original Kibble counting which uses one additional point with random field asignment inside each of the two triangles which constitute the elementary square lattice cell. We consider the identification of ξ with the lattice constant for a random assignment of field vectors to each vertex of the square lattice as the natural definition of the correlation length.

This basic setup opens a wide variety of dynamical situations for systematic investigation. As just one example we shall discuss here only the case of a linear quench in the scale parameter λ

$$\lambda=\lambda_i+\frac{\lambda_f-\lambda_i}{t_Q}\ t\quad (0\leqslant t\leqslant t_Q) \tag{14}$$

with $\lambda_i\gg 1$ and $\lambda_f\ll 1$. Starting from the initial random set, at the beginning of the quench a large value of λ_i attempts to establish long range order with very small values of the local winding density ρ. When λ approaches values aound $\lambda\approx 3$ to 1, individual defects start to be formed out of this more or less organized low-density soup. Near the end of such a quench, for very small λ we expext an ensemble of N_+ defects and N_- antidefects each essentially localized on a single lattice cell. For $t>t_Q$ the evolution can still be continued with $\lambda=\lambda_f$ to allow for final stabilization of the defects formed, or for possible mutual annihilations on a much longer time scale.

After the onset of the quench ordering of the configurations proceeds within typical relaxation times τ and the extent to which the ordering can spread before the local defects appear is governed by the ratio τ/t_Q, which is the appropriate measure for the quench velocity. For a fast quench we expect the final defect density to be close to our modified Kibble limit discussed above, because most of the initial random (incomplete) winding will directly evolve into complete local 4π winding. For slow quenches the random winding will have time to be smoothed away into large areas of low winding density, before finally a few defects and antidefects reappear.

This naturally provides the appropriate setting to investigate formation and size of DCC domains. There is, however, a severe limitation to this discussion, also within the model (13): The stabilization mechanism of the baby skyrmions relies on a strong symmetry breaker, the last term in Eq. (13). This term prevents formation of large areas of aligned but randomly oriented field configurations if we consider the complete field vectors $\hat{\Phi}$. In the spatial domains outside the range of the topological defects the field will essentially be aligned in $\hat{e}_3$ direction. Still, a partial aspect of DCC formation can be studied: In the so called ''easy plane'' orthogonal to $\hat{e}_3$, the field components Φ_1 and Φ_2 can freely align in random directions and the partial correlation function

$$C(|2-1|)=\langle\cos\phi(1)\cos\phi(2)+\sin\phi(1)\sin\phi(2)\rangle \tag{15}$$

(where the arguments 1,2 stand for two arbitrary lattice

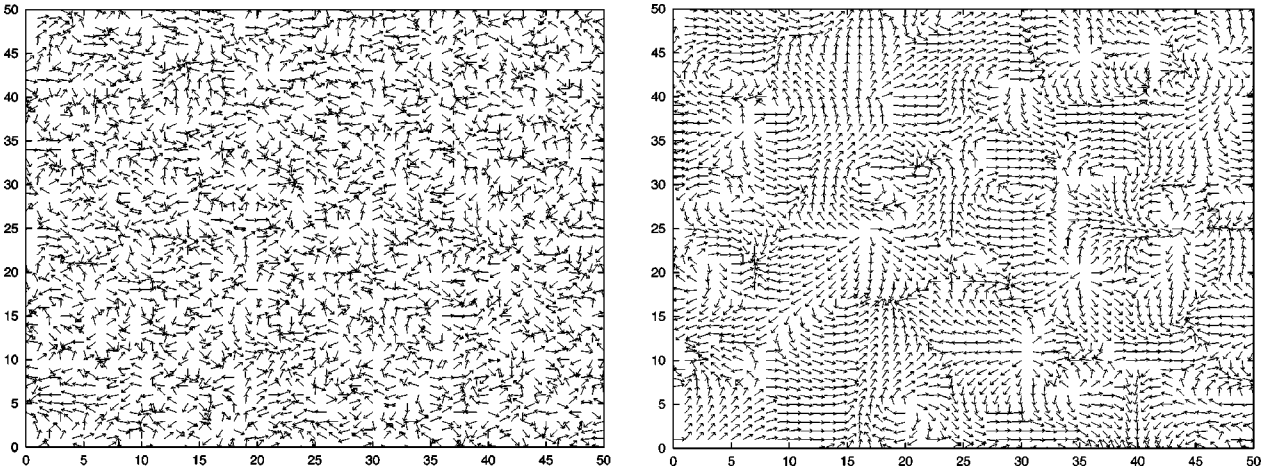

FIG. 3. Φ field projected into (and renormalized in) the easy plane for (a) fast ($t_Q=10$) and (b) slow ($t_Q=200$) quench near $\lambda\approx 3$.

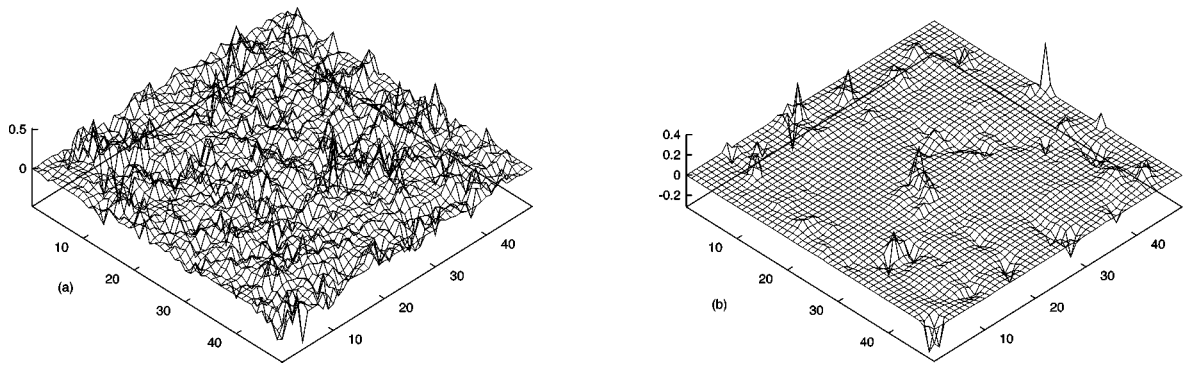

FIG. 4. Winding density ρ during (a) fast ($t_Q=10$) and (b) slow ($t_Q=200$) quench near $\lambda\approx 3$.

points) provides the information about the size of aligned domains. It should, however, be noted that the aligning force in the easy plane due to the first term in Eq. (13) (the nearest neighbor interaction) is active only in areas where $\sin\theta\neq 0$. This means that the formation of DCC domains can only be studied during the early parts of the quench where the strength of the symmetry breaker is not yet sufficient to form small localized defects with strictly aligned (in $\hat{e}_3$ direction) domains in between. As soon as these local defects appear (around $\lambda<3$) the disoriented aligned areas in the easy plane begin to rerandomize due to thermal fluctuations. So, the formation of DCC domains is closely connected to small but nonvanishing winding density, which by itself is an interesting aspect.

In the following we describe some results of numerical simulations on a 51×51 lattice with an ensemble of random initial configurations which, however, have been selected as to satisfy $B=0$. Of course, other values of B can be selected to study a possible influence of the total winding number. The algorithm conserves B as discussed above. For illustration we present two intermediate steps in the evolution of one specific arbitrary configuration during a fast quench ($t_Q=10$ time steps) and a slow quench ($t_Q=200$ time steps).

The first set shows the situation shortly before $\lambda(t)$ crosses the value of $\lambda\approx 3$, i.e., just before localized defects begin to form. The corresponding correlation functions (15) in Fig. 2 indicate that the ordering in the easy plane has hardly progressed beyond one lattice unit during the fast quench, while it extends beyond five lattice units after the slow quench. This becomes very evident if we look (in Figs. 3) at the field Φ projected into the easy plane and normalized to unity in the easy plane (i.e., the components of the arrows in the plot simply are $\cos\phi$ and $\sin\phi$). This provides an instant view of DCC domains and defects and it shows that for the fast quench a high density of nascent defects leaves no space for large aligned domains while during the slow quench a well-developed DCC pattern emerges. The corresponding winding density distributions ρ display a rough surface [Fig. 4(a)] versus essentially smooth areas of low density with few emerging local spikes [Fig. 4(b)]. Finally, Fig. 5 shows the resulting ensemble of defects shortly after the end of the quench where λ has reached its final value of $\lambda_f=0.1$ and the local defects have stabilized. Counting the final number of defects and antidefects which evolve from this particular initial configuration we find $N_+=N_-=46$ for the fast ($t_Q=10$) quench and $N_+=N_-=15$ for the slow ($t_Q=200$) quench.

Evolving $\mathcal{N}=50$ randomly chosen (but selected for $B=0$) initial configurations through the quench (14) leads to an ensemble of defects and antidefects for each quench time t_Q as shown in Fig. 6. The modified Kibble limit as discussed above for the square lattice is $N_++N_-\rightarrow(50\times 50)/16\approx 156$. The boundary conditions ($\theta=0$) reduce this value to about 144 for this lattice size. For the sudden quench ($t_Q=0$) the measured numbers approach a mean value of only about 133 due to a few instant annihilations. For increasing quench time the defect numbers drop to a mean value of about 32 near $t_Q=200$ as indicated by the full

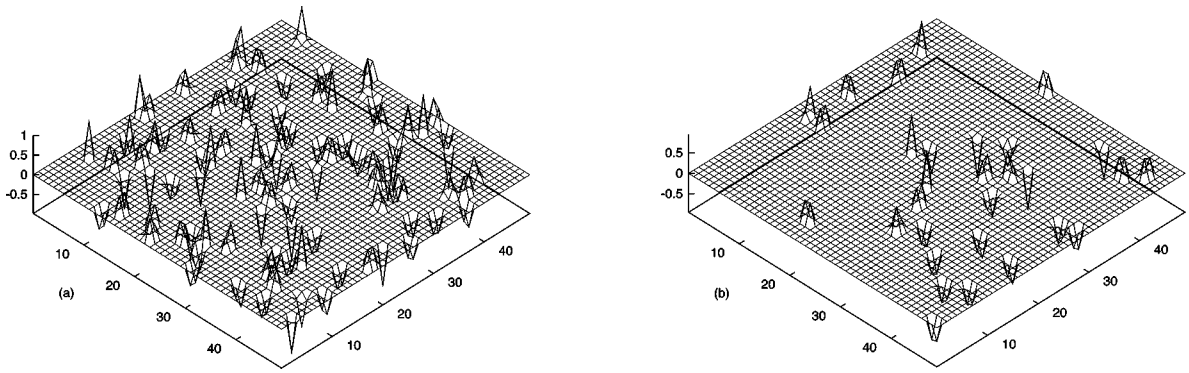

FIG. 5. Final winding density ρ after (a) fast ($t_Q=10$) and (b) slow ($t_Q=200$) quench at $\lambda=0.1$. The resulting (anti)defect numbers are $N_+=N_-=46$ and $N_+=N_-=15$ in cases (a) and (b), respectively.

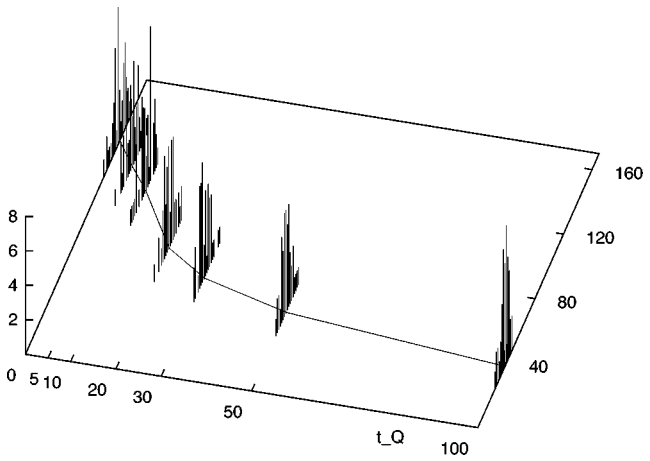

FIG. 6. Final defect plus antidefect multiplicities for different quench times t_Q; their average values are connected by the full line.

line in Fig. 6 which connects the mean values for the different quench times. The root mean square deviation from the average values decreases from about $\Delta \approx 10$ for the sudden quench to $\Delta \approx 5$ near $t_Q = 200$. Of course, these details depend on the specific choice of the quench mechanism used here. For applications to specific physical situations the appropriate temperature dependence of the effective action and temporal structure of the quench has to implemented.

IV. CONCLUSION

The purpose of this paper is to study the influence of the spatial extent of topological defects on their formation during a dynamical quench in a symmetry breaking phase transition. Apart from the combinatorial factors of the Kibble mechanism it is the ratio of the momentaneous magnitude of the winding length l_W (as determined by the temperature dependent effective classical Lagrangian) to the correlation length ξ near T_c which is essential for the resulting multiplicities of defects and antidefects. This leads to a crucial role of the quench time on the scale of the relaxation time τ typically needed for defect formation. If during the early part of the quench the winding length is large on the scale of ξ, the resulting defect multiplicities are much reduced as compared to the combinatorial Kibble limit for pointlike defects.

As illustration we presented numerical simulations in the nonlinear $1D$-O(2) and $2D$-O(3) models which are characterized by a topologically conserved winding number B, in view of applications where this number corresponds to a physically relevant observable. For the lattice simulation it is essential to implement the geometrical meaning of the winding density for the discrete map. Then boundary conditions on angular variables still serve to enforce integer values for B, although topological arguments for B conservation no longer apply. However, by explicit control during the evolution B-violating steps can be excluded. If conservation of B is an important feature of the physical system under discussion, like baryon number conservation in chiral meson field models, extensions to the linear versions of O(N) models have to include the additional degree of freedom in the form of a modulus variable in an $S^{N-1} \times R^1$ embedding. For comparison we have briefly discussed the topologically trivial R^2-embedding of the linear O(2) model. Unfortunately, in these low-dimensional models, the winding length of defects is closely tied to explicit symmetry breaking. This leads to a dramatic difference between Euclidean and angular embedding if the symmetry breaking is sufficiently strong to destabilize nontrivial configurations. The same feature also hampers the investigation of DCC domains in these low-dimensional models. It is only in the easy plane of the O(3) model where partial aspects of randomly oriented alignment can be observed. It has been argued that the bias introduced into the ensemble of initial configurations (for $T > T_c$) by explicit symmetry breaking causes another drastic reduction of defect multiplicities. This interesting aspect has been omitted here, again for the same reason that the symmetry breakers simultaneously have to serve as stabilizers for the defects.

Of course, the real challenge is the formation of $3D$-O(4) skyrmions as a nonperturbative model of how baryons emerge in the cooling of the hot meson soup. In that model stabilization of defects and explicit symmetry breaking through small mesonic masses are almost unrelated. Therefore all the interesting features concerning winding length, formation of DCC domains, effects of the modulus field, baryon number conservation, bias in the initial ensemble, all can be studied quite independently with the same methods used here for baby skyrmions.

ACKNOWLEDGMENTS

The author would like to thank J. Klomfass, J. Dziarmaga, and B.A. Ivanov for interesting discussions.

[1] See, e.g., G.E. Volovik, *Exotic Properties of Superfluid He^3 (World Scientific, Singapore, 1992); M. Hindmarsh and T.W.B. Kibble, Rep. Prog. Phys.* **58**, 477 (1995); A.D. Rutenberg and A.J. Bray, Phys. Rev. Lett. **74**, 3836 (1995); W.H. Zurek, Phys. Rep. **276**, 177 (1996); R.H. Brandenberger, Pramana, J. Phys. **51**, 191 (1998).

[2] T.H.R. Skyrme, Proc. R. Soc. London **A260**, 127 (1961); E. Witten, Nucl. Phys. **B223**, 422 (1983); **B223**, 433 (1983).

[3] T.A. DeGrand, Phys. Rev. D **30**, 2001 (1984); J. Ellis and H. Kowalski, Phys. Lett. B **214**, 161 (1988); J. Ellis, U. Heinz, and H. Kowalski, *ibid.* **233**, 223 (1989); J. Ellis, M. Karliner, and H. Kowalski, *ibid.* **235**, 341 (1990).

[4] J.I. Kapusta and A.M. Srivastava, Phys. Rev. A **52**, 2977 (1995).

[5] P. Gerber and H. Leutwyler, Nucl. Phys. **B321**, 387 (1989).

[6] S. Weinberg, Physica A **96**, 327 (1979); J. Gasser and H. Leutwyler, Ann. Phys. (N.Y.) **158**, 142 (1984).

[7] R. Pisarski and F. Wilzcek, Phys. Rev. D **29**, 338 (1984).

[8] A. Kocic and J. Kogut, Nucl. Phys. **B455**, 229 (1995).
[9] A.A. Anselm, Phys. Lett. B **217**, 169 (1988); A.A. Anselm and M.G. Ryskin, *ibid.* **266**, 482 (1991); J.P. Blaizot and A. Krzywicki, Phys. Rev. D **46**, 246 (1992); *ibid.* **50**, 442 (1994); J.D. Bjorken, Int. J. Mod. Phys. A **7**, 4189 (1992); Acta Phys. Pol. B **23**, 561 (1992); ''Disoriented chiral condensate,'' Proceedings of the Workshop on Continuous Advances in QCD, Minneapolis, 1994, SLAC-PUB-6488 (1994); S. Gavin, Nucl. Phys. **A590**, 163c (1995).
[10] A.M. Polyakov, *Gauge Fields and Strings* (Harwood, Academic, Chur, Switzerland, 1987).
[11] K. Rajagopal and F. Wilczek, Nucl. Phys. **B399**, 395 (1993), **B404**, 577 (1993); S. Gavin, A. Gocksch, and R.D. Pisarski, Phys. Rev. Lett. **72**, 2143 (1994); K. Rajagopal, in *Quark-Gluon Plasma 2*, edited by R. Hwa (World Scientific, Singapore, 1995); M.A. Lampert, J.F. Dawson, and F. Cooper, Phys. Rev. D **54**, 2213 (1996); J. Randrup, Nucl. Phys. **A616**, 531 (1997); Phys. Rev. D **56**, 4392 (1997).
[12] G. Holzwarth, Phys. Rev. D **57**, 3749 (1998).
[13] J.I. Kapusta and A.P. Vischer, Z. Phys. C **75**, 507 (1997).
[14] T.W.B. Kibble, J. Phys. A **9**, 1387 (1976).
[15] N.H. Christ, R. Friedberg, and T.D. Lee, Nucl. Phys. **B202**, 89 (1982).
[16] W.H. Zurek, Nature (London) **317**, 505 (1985); P. Laguna and W.H. Zurek, Phys. Rev. Lett. **78**, 2519 (1997).
[17] H. Walliser, Phys. Rev. D **56**, 3866 (1997).
[18] J. Dziarmaga, Phys. Rev. Lett. **81**, 5485 (1998); J. Dziarmaga and M. Sadzikowski, hep-ph/9809313.
[19] B.M.A.G. Piette, H.J.W. Müller-Kirsten, D.H. Tchrakian, and W.J. Zakrzewski, Phys. Lett. B **320**, 294 (1994); B.M.A.G. Piette, B.J. Schroers, and W.J. Zakrzewski, Z. Phys. C **65**, 165 (1995); Nucl. Phys. **B439**, 205 (1995).
[20] M. Zapotocky and W.J. Zakrzewsky, Phys. Rev. E **51**, R5189 (1995); A.D. Rutenberg, W.J. Zakrzewsky, and M. Zapotocky, Europhys. Lett. **39**, 49 (1997).
[21] R.S. Ward, Lett. Math. Phys. **35**, 385 (1995).
[22] M. Lüscher, Nucl. Phys. **B200**, 61 (1982).